JOURNAL OF ENERGY SYSTEMS

2025, 9(4)

2602-2052 DOI: 10.30521/jes.1756747 Research Article

Simultaneous integration of photovoltaic distributed generation and distribution static compensators for technical performance enhancement in distribution networks using PSO with velocity pausing and adaptive strategy

Youcef Kachaou
University of Brothers Mentouri-Constantine 1, Constantine, Algeria, youcef.kachaou@lec-umc.org
Manel Bidi *
University of brothers Mentouri-Constantine 1, Constantine, Algeria, bidi_manel@yahoo.fr
Ishak Aloui
University of brothers Mentouri-Constantine 1, Constantine, Algeria, ishakaloui486@gmail.com

Submitted: 02.08.2025
Accepted: 02.12.2025
Published: 31.12.2025

* *Corresponding Author*

Abstract: The simultaneous integration of Distributed Generations (DGs) and Distribution Static Compensator (DSTATCOM) improves the operation of distribution systems and introduces multiple technical dimensions. The paper proposes a procedure for optimal integration of Photovoltaic Distributed Generation (PVDG) and Distribution Static Compensator (DSTATCOM) in Radial Distribution Systems (RDSs). The procedure is formulated as a composite objective function (COF). From the technical point of view, total active power losses (TAPL), total voltage deviation (TVD), voltage stability index (VSI), and voltage profile improvement level are considered. The method consists of a hybrid improvement technique combining velocity pausing and adaptive strategy (VAS) with a so-called PSO algorithm to enhance the solution quality of the proposed algorithm in comparison with other algorithms mentioned in the literature. The efficiency of the method is examined for 3 cases with a test setup having IEEE 33-bus and 69-bus RDSs. According to tests, the hybrid VAS-PSO algorithm shows that the simultaneous allocation of multiple PVDG and DSTATCOM in all standard test systems significantly achieves the lowest COF value (reduces the TAPL and TVD and enhances the voltage profile and VSI Compare) and presents better performance than the other tested algorithms. Besides, that the ability to allocate PVDG and DSTATCOM optimally while maintaining a voltage profile level within the permissible limit, where the TAPL and TVD decreased to 94.43% and 91.45%, respectively under the IEEE 33 bus and to 97.96% and 93.16% for the IEEE 69 bus is achieved for various scenarios using the proposed hybrid VAS-PSO algorithm.

Keywords: *Distributed generation, DSTATCOM, Photovoltaic network, TAPL, TVD, VAS-PSO algorithm*

Cite this paper as: Kachaou Y, Bidi M, Aloui I., Simultaneous integration of photovoltaic distributed generation and distribution static compensators for technical performance enhancement in distribution networks using PSO with velocity pausing and adaptive strategy. *Journal of Energy Systems 2025; 9*(4): 380-404, DOI: 10.30521/jes.1756747

2025 Published by peer-reviewed open access scientific journal, JES at DergiPark (https://dergipark.org.tr/jes)

Nomenclature	
RDS	Radial distribution network
PVDG	Photo-Voltaic Distributed Generation
DSTATCOM	Distribution Static Compensator
TVIC	Time Varying Inertia Coefficients
VAS	Velocity pausing and Adaptive Strategy
TVD	Total Voltage Deviation
VSI	Voltage Stability Index
TAPL	Total Active Power Losses
COF	Composite Objective Function

1. INTRODUCTION

The global energy sector is undergoing a profound transformation, shifting from traditional fossil fuel-based generation to renewable energy sources (RES), driven by the increasing demand for electricity, concerns about greenhouse gas emissions, and the need for long-term sustainable energy strategies [1]. Unlike traditional centralized methods that rely on thermal power plants, which contribute to high carbon emissions and power loss during transmission (often ranging between 5% and 10% globally), the integration of RES promotes decentralized and sustainable production near consumption points, reducing environmental impact and enhancing energy security [2,3]. According to the International Energy Agency (IEA), renewable capacity additions reached over 300 GW in 2023, with Photovoltaic Distributed Generation (PVDG) systems accounting for more than 60% of this growth. A recent report from the International Renewable Energy Agency (IRENA) says that solar energy will make up 25% of the world's electricity generation by 2050. PVDG units provide local generation, reducing transmission power losses and making the grid more reliable. Therefore, they are increasingly used in Radial Distribution Systems (RDS) due to their modular nature, decreasing costs, and environmental benefits and reduce system losses, enhance reliability, and support voltage regulation when properly integrated [4,5]. Despite these benefits, increasing penetration levels of PVDG in RDS provide several operational issues. The intermittent nature of solar energy results in variable power injections, which can lead to voltage deviations, reverse power flows, and reduced efficacy in conventional voltage regulation equipment [6,7]. These fluctuations have a negative impact on power quality and grid stability and place stress on line capacity. This behavior contributes to increased total active power losses, which is an increasingly important problem in RDS with high R/X ratios. Therefore, effective planning and control strategies are necessary to ensure that PVDG integration enhances rather than degrades the performance of distribution networks [8]. Meanwhile, in the presence of PVDG in RDS, Distribution Static Synchronous Compensators (DSTATCOMs) have emerged as a vital technology for overcoming these challenges. They offer dynamic voltage regulation and reactive power compensation capabilities. These functions are achieved by injecting or absorbing reactive power, thereby enhancing grid performance, minimizing voltage variation, improving power quality and the voltage deviation coefficient, and optimizing the power factor. It also enables the installation of a higher number of PVDGs [9]. Improper sizing and allocation of PVDG and DSTATCOM can increase power system losses and reduce voltage profiles, thereby deteriorating the system's capacity. Therefore, integrating PVDG with DSTATCOM in the most optimal way possible provides many benefits for the distribution system, including enhancing power quality, expanding system capacity, and managing power demand according to Ref. [10].

The research aims to evaluate the energy performance and voltage profiles of networks incorporating DSTATCOMs and PVDG systems, emphasizing the impact of their combined use on system reliability and efficiency. By investigating this simultaneous integration, the study seeks to answer several key research questions. For example:

How does the joint deployment of DSTATCOMs and PVDG systems affect power losses and voltage stability in RDS?

What are the optimal configurations and operational strategies for these technologies to maximize their performance?

Can this integration provide scalable solutions for future grids with higher levels of renewable energy penetration?

The problem of optimally integrating PVDG and DSTATCOM stations into RDS has been widely studied in specialized literature. However, despite the promising potential of DSTATCOMs and PVDG

systems, most studies have focused on their individual applications rather than their simultaneous integration. Furthermore, the interaction between these technologies and their role in addressing emerging distribution system challenges, such as the increasing proliferation of distributed generation and the need for adaptive energy management strategies, remains unclear. Closing this knowledge gap is crucial for improving the performance of modern RDS and facilitating the transition to renewable energy systems.

The following is an overview of some of the latest developments in this area of research. It presents optimization algorithms developed by researchers to determine the optimal simultaneous allocation and sizes of PVDG and DSTATCOM units in an RDS system [11]. Ref. [12] presents a new optimization technique for the locations and sizes of DGs and DSTATCOMs in an RDS based on a multi-objective approach. It uses black widow optimization (BWOA) to improve voltage profile and power loss reduction. In Ref. [1], the hybrid improvement methods combining the Firefly Algorithm (FA) and PSO algorithms with different acceleration coefficients are presented to enhance the overall solution quality of these hybrid algorithms. By doing it, the paper aimed to integrate PVDG panels and DSTATCOMs in the RDS, optimally while improving the active power loss level (*APLL*), voltage deviation level (*VDL*), net savings level (*NSL*), and environmental pollution reduction level (*EPRL*). In Ref. [4], a modified version of the homonuclear molecule optimization (mHMO) method was developed to determine the optimal allocation and sizing of PVDG and DSTATCOM in two standard IEEE 33-bus and 69-bus systems, while minimizing a multi-objective function (MOF) based on total active power losses (*TAPL*), total voltage deviation (*TVD*), and the investment cost of the integrated devices (ICPVDG and ICDSTATCOM). The approach proposed in Ref. [13] aims to achieve the optimal location and size of PVDGs and DSTATCOMs in RDS by focusing on reducing the investment and operating costs associated with PVDGs and DSTATCOMs as an objective function. The proposed methodology combines a discrete-continuous version of the multiverse optimization (MVO) algorithm with a matrix power flow method based on successive approximation (MAX). Ref. [14] presents the planning of an optimal PVDG system and a DSTATCOM device with network reconfiguration (NRX), using a hybrid marine predator jellyfish algorithm (HMPJA). This improves voltage deviation, reduces total power loss, and boosts efficiency, ultimately raising system stability. The work presented by Ref. [15] proposes a new methodology based on a metaheuristic optimization algorithm inspired by nature, known as the Whale Optimization Algorithm (WOA). The objective function of the proposed method is to minimize the total power losses and total operating costs of DG and DSTATCOM in RDS by determining the optimal positioning and size of DGs and DSTATCOM through the loss sensitivity factor and WOA. In Ref. [11], the Fuzzy-Light Search (FLSA) algorithm was proposed to reduce total power loss and improve voltage profile in radial distribution systems by solving the optimal placement problem of DSTATCOM and PVDG in RDS. In other work [16], the improved gray wolf optimizer (I-GWO) algorithm model was applied to minimize total active power losses and improve the expected voltage profile in the RDS. The power optimization issue was achieved by determining the optimal distribution and size of DSTATCOM stations while taking into account system constraints, such as the intermittent and random nature of loads and renewable energy resources (especially wind and solar energy). In Ref. [17], the Water Cycle Algorithm (WCA) was proposed to determine the optimal locations and sizes of distributed generating units and capacitor banks. The proposed method aims to deliver technical, economic, and environmental benefits. It considers various objective functions, such as minimizing power losses, voltage deviation, total electricity cost, and total emissions from generation sources, as well as improving the voltage stability index. In Ref. [18], a Bacterial Foraging Optimization Algorithm (BFOA) with a Loss Sensitivity Factor (LSF) was proposed for determining the optimal size and location of distributed generation (DG) and static synchronous compensators (DSTATCOM) in a radial distribution system simultaneously. The objective function was formulated to minimize energy loss and operating costs while optimizing the system's voltage profile subject to equality and inequality constraints. In Ref. [19], a novel approach was proposed for determining the optimal locations and sizes of DG and DSTATCOM in RDS, with the aim of minimizing total power losses in these RDSs subject to equality and inequality constraints. The voltage stability index (VSI) was also enhanced through the application of a cuckoo search algorithm (CSOA). In Ref. [20], Elite Harris Hawks Optimization (EHHO) algorithm is presented as an effective method for calculating the optimal size of photovoltaic cells and static distribution compensators (DSTATCOM), as well as determining their ideal placement

within distribution systems. The multi-objective function involves minimizing energy loss and improving both the voltage pattern and voltage stability in distributed power generation. In Ref. [21], the Dwarf Minimizer Optimization (DMO) method is used to determine the optimal size of DG and DSTATCOM in RDS. The proposed method takes an integrated approach to loss sensitivity factors and Dwarf Mongoose Optimization, determining the optimal locations and sizes of DG and DSTATCOMs to reduce energy loss, improve the voltage profile, and minimize operating costs. The work in Ref. [22] proposes a hybrid teaching-learning-based optimization-particle swarm optimization (TLBO-PSO) algorithm to achieve optimal DG and DSTATCOM configurations. A multi-objective function was developed to optimize DG and DSTATCOM configurations in an IEEE 33 RDS, aiming to maximize cost-benefit and voltage stability while minimizing network security and total power losses. As seen from the literature above, a diversity of optimization issues exists for many different applications.

The current paper presents a new approach for the optimal integration of simultaneous PVDG and DSTATCOM into RDS using PSO algorithms based on velocity pausing and adaptive strategy, (VAS-PSO) while considering a composite objective function (*COF*) based on total active power losses, voltage deviation, and voltage stability index. The proposed algorithm has a potential to enhance the capacity to solve complex optimization problems and to attain a better balance between exploration and exploitation. Initially, the algorithm employs a time-varying inertia coefficient (*TVIC*) allowing to converge faster and searching for the best solution. Secondly, the proposed algorithm uses velocity-pausing techniques to address the common limitation of classical particle swarm algorithms, namely premature convergence. This limitation often causes performance issues in complicated applications. A random selection strategy is used for the velocity-pausing factor "a" which is valued between 0 and 1, to eliminate infeasible solutions. In addition, the current algorithm uses an "adaptive strategy", which is a clever way of dynamically balancing exploration and exploitation to make it work better. The fourth item is that the current algorithm works on a concept called "symmetric cooperative swarms", where it treats different particles in different ways to help find the best solutions. Finally, a terminal replacement mechanism is implemented for getting rid of the particles that are performing the worst and makes the algorithm more accurate and effective as in Ref. [23]. The proposed algorithm aims to reduce the total active power loss (*TAPL*) and total voltage deviation (*TVD*), in addition to the improvement of the voltage profile and voltage stability index (VSI). The algorithm is applied to the IEEE 33 and 69 standard RDS systems in four case studies. This research paper made several important contributions. These can be summarized as follows:

Propose a new version of the PSO algorithm based on the velocity pausing coefficient and an adaptive strategy to solve the problem of optimizing the integration of PVDG and DSTATCOM sources in a radial distribution network.

Validate the performance of the proposed algorithm by applying it to two standard IEEE 33 and 69 buses and achieving substantial technical improvements to the composite objective function (COF).

Confirmation of the ability of the proposed algorithm to allocate optimally hybrid PVDG and DSTATCOM devices to improve the performance of RDS in different case studies.

The next sections of the paper are organized as follows: Section 2 formulates the optimal allocation problem for the location and sizing of PVDG and DSTATCOMs in RDS, defined by the composite objective function (*COF*) for minimizing power loss and total voltage deviation. Section 3 describes the hybrid VAS-PSO algorithm proposed to solve the mathematical formulation, as well as the optimization parameters used. Section 4 presents the simulation results and discussion with a comparison between the other techniques. Consequently, last Section lists the main conclusions and future research related to this work.

2. PROBLEM FORMULATION AND CONSTRAINTS

2.1. Objective Function

The Composite Objective Function (*COF*) was created to determine the best size and placement of both PV-DG and DSTATCOM units inside RDS. The OF aims to reduce the parameters of *TAPL* and *TVDI*:

$$COF = min\ (TAPL + TVD) \tag{1}$$

$$TAPL = \sum_{i=1}^{Nb} P_{loss}(i, i+1) \tag{2}$$

where, *Nb* denotes the total number of branches in RDS. The active power loss of the line branch P_{loss} is described by,

$$P_{loss(i,i+1)} = \left(\frac{P_{i,i+1}^2 + Q_{i,i+1}^2}{|V_i|^2}\right) R(i, i+1) \tag{3}$$

where, $R_{(i,i+1)}$ are the resistance of branch. $P_{(i,i+1)}$ and $Q_{(i,i+1)}$ represents active and reactive powers of the line branches between buses *i* and *i+1* in the RDS. V_i represent the voltage at bus *i*. For the *TVDI* according to Refs. [2,24] we can determine as,

$$TVD_j = \sum_{j=2}^{N_{bus}} |1 - V_j| \tag{4}$$

Different measures are used to assess how safe power systems are. One key sign is the VSI, which checks how stable the voltage is at each point in the system. It looks at how power flows and the nodes that are more likely to have voltage problems. It can be defined as, according to Ref. [25]:

$$VSI(i+1) = |V_{i+1}|^4 - 4\left[P_{i,i+1} X_{i,i+1} - Q_{i,i+1} R_{i,i+1}\right]^2 - 4\left[P_{i,i+1} R_{i,i+1} + Q_{i,i+1} X_{i,i+1}\right]|V_{i+1}|^2 \tag{5}$$

2.2. Constraints of Equality

The active and reactive power balances of the assessed power system are expressed as equality constraints in Eqs. (6) and (7) according to Refs. [26,27]. The total active power and total reactive power provided by the substation matches the necessary active and reactive power demand and associated losses along with that generated by PV-DG and DSTATCOM devices and they are given as,

$$P_G + P_{PV-DG} = P_D + P_{loss} \tag{6}$$

$$Q_G + Q_{DSTATCOM} = Q_D + Q_{loss} \tag{7}$$

where, P_G, Q_G are represent the total active and reactive power of the generator, P_D and Q_D stand for the total active and reactive power of the demand load, P_{PV-DG} and $Q_{DSTATCOM}$ denote the total active power injection from the PV-DG and the total reactive power injection from the DSTATCOM.

2.3. Constraints of Inequality

2.3.1. Distribution line constraints

Bus voltage limits are given by,

$$V_{min} \leq |V_i| \leq V_{max}, \tag{8}$$

and voltage drop limits are defined by,

$$|1 - V_i| \leq \Delta V_{max}. \quad (9)$$

The line capacity limit is represented by,

$$|S_{i,i+1}| \leq |S_{max}| \quad i = 1, \ldots, n, \quad (10)$$

where, V_{min} and V_{max} are indicative of the specified voltage limits and ΔV_{max} represents the maximum voltage drops. $S_{i,i+1}$ and S_{max} represent the apparent power in the branch and the maximum apparent power, respectively.

2.3.2. PV-DG and DSTATCOM units limits

The limits production of the PV-DG and DSTATCOM stations are articulated using disparity constraints. These may be expressed as in Refs. [26-29]:

$$Q_{DSTATCOM}^{min} \leq Q_{DSTATCOM} \leq Q_{DSTATCOM}^{max} \quad (12)$$

$$P_{PV-DG}^{min} \leq P_{PV-DG} \leq P_{PV-DG}^{max} \quad (11)$$

where, P_{PV-DG}^{min}, P_{PV-DG}^{max} and $Q_{DSTATCOM}^{min}$, $Q_{DSTATCOM}^{max}$ represent the active and reactive power output capacity limits of PV-DG and DSTATCOM, respectively in RDS. Note that the power components satisfy,

$$\sum_{i=1}^{N_{PV-DG}} P_{PV-DG}(i) \leq \sum_{i=1}^{N_{bus}} P_D(i) \ , \quad (13)$$

$$\sum_{i=1}^{N_{DSTATCOM}} Q_{DSTATCOM}(i) \leq \sum_{i=1}^{N_{bus}} Q_D(i) \ , \quad (14)$$

where P_{PV-DG} $Q_{DSTATCOM}$, represent the total injected active and reactive power in RDS and should be less than the total active and reactive of demand P_D and Q_D.

$$2 \leq PV - DG_{location} \leq N_{bus} \ , \quad (15)$$

$$2 \leq DSTATCOM_{location} \leq N_{bus} \ , \quad (16)$$

where $PV - DG_{location}$ and $DSTATCOM_{location}$ represent the Position of PV-DG and DSTATCOM stations in RDS and are allowable only from the bus number 2.

$$N_{PV-DG} \leq N_{PV-DG\,max} \ , \quad (17)$$

$$N_{DSTATCOM} \leq N_{DSTATCOM\,max} \ , \quad (18)$$

Where $N_{PV-DG}, N_{DSTATCOM}$ represent the number of PV-DG and DSTATCOM stations and $N_{PV-DG,max}$, $N_{DSTATCOM,max}$ represent Maximum number of PV-DG and DSTATCOM stations in RDS.

$$N_{PV-DG,i}/location \leq 1, \quad (19)$$

$$N_{DSTATCOM,i}/location \leq 1 \ , \quad (20)$$

$N_{PV-DG,i}$, $N_{DSTATCOM,i}$ represent the emplacements of PV-DG and DSTATCOM stations on the bus i Eqs. (19) and (20) refer that only one PV-DG or DSTATCOM device is permitted in one location.

3. DESCRIPTION OF THE PROPOSED ALGORITHM

3.1. PSO Algorithm

PSO is an algorithm inspired by natural phenomena, and it draws upon the principles of swarm intelligence to tackle various optimization problems. The method draws inspiration from the way birds collectively search for food. The principal objective of PSO is to enhance search processes through the emulation of the coordinated movements exhibited by particles within a swarm. In this framework, each particle represents a possible solution and moves around the search space by changing its position and speed. These adjustments are influenced by the particle's personal experiences as well as the information shared by other members of the swarm. The particle positioning suggests a potential solution, whilst its velocity indicates the pace and direction of its pursuit for enhanced solutions.

Firstly, the search space is evenly filled with particles, each with its own speed. A fitness function is used to judge their performance. This lets us change both the best position that each particle has found the individual best and the best position that the whole swarm has found the global best. As the algorithm moves forward, particles keep changing their speeds and positions, leveraging their individual best outcomes and the collective findings of the swarm to pursue optimal solutions [30]. The mathematical equations that govern the updates to the particle velocity and position are outlined as following:

$$V(t+1) = w\,V(t) + C_1\,rand\left(P_{best} - X(t)\right) + C_2 rand\left(G_{best} - X(t)\right) \quad (21)$$

$$X(t+1) = X(t) + V(t+1) \quad (22)$$

Here, the coefficient $V(t)$ denotes the particle velocity on time t, $X(t)$ signifies the particle position, $C_1$and C_2 are the coefficients of acceleration. $rand$ denotes a collection of randomly chosen numbers that are uniformly distributed across the interval from 0 to 1, P_{best} denotes the optimal individual particle position, G_{best} indicates the global optimal position of the group, and w represents the inertia weight, which is given by,

$$w(t) = (w_{max} - w_{min})\left(\frac{T-t}{T}\right) + w_{min}, \quad (23)$$

where w_{max} and w_{min} are the highest and lowest values of the inertia weight, respectively. T is the maximum number of iterations, and t is the current iteration.

3.2. VAS-PSO Algorithm

The suggested methodology aims to enhance the optimization efficacy of PSO through the integration of velocity pausing and adaptive strategy according to Ref. [23].

3.2.1. Time-varying inertia weight

Modifying the inertia weight is an important feature of the particle swarm optimization (PSO) technique that considerably improves its efficacy. Initially, velocity pausing was meant to improve PSO global search capabilities while preventing premature convergence to local optima. However, while this method can improve exploration, it can also cause delays and, in some situations, long term convergence difficulties. To address these issues, a time decreasing weight function is frequently employed to adjust the inertia weight, particularly in the last stages of execution. This function is intended to lower the inertia weight gradually over iterations while retaining powerful global search capabilities and promoting faster convergence to the ideal solution. By dynamically modifying the inertia weight, PSO achieves a better balance between exploration and exploitation, optimizing both convergence speed and total global search performance [31]. The following equation shows how to determine the weight of inertia,

$$w(t) = exp^{-\left(\frac{bt}{T}\right)^b} \tag{24}$$

Here T represents the maximum number of iterations, whereas b denotes the constant value.

3.2.2. Velocity pausing

This paper introduces the innovative concept of velocity pausing, in which each particle is not required to update its velocity at each iteration. In other words, a particle is allowed to travel at the same speed as in the preceding iteration. This notion allows particles to move at three possible speeds: Slower, faster, and constant. This differs from the typical PSO method, in which particles move exclusively at faster or slower rates. The fundamental advantage of velocity pausing is that it introduces a third movement option (constant speed), which can help balance exploration and exploitation while avoiding the severe premature convergence of standard PSO [31]. The mathematical relationship for the velocity pauses equation is presented as follows:

$$\begin{gathered} V_i(t+1) = V_i(t) \quad if\ rand\ < \alpha \\ V_i(t+1) = w(t)V(t) + C_1\, r_1\, \left(P_{best_i} - X_i(t)\right) + C_2 r_2\, \left(G_{best_i} - X_i(t)\right) Otherwise \end{gathered} \tag{25}$$

Here, "a" is the velocity pausing parameter. If the pause parameter a is greater than 1, all particles will change their velocities at each iteration in the same way that the classical PSO algorithm does. This circumstance is undesirable because velocity halting may occur. In contrast, an excessively low value of a forces particles to move at a constant pace, preventing them from moving faster or slower. As a result, selecting the appropriate value of a is critical for attaining balanced velocity pausing, which can contribute to peak performance. To aid PSO in avoiding premature convergence, the velocity equation of the typical PSO algorithm is modified by modifying the first velocity term and removing the inertia weight component. The formula for updating the particle position is as follows:

$$\begin{gathered} X(t+1) = G_{best} + w\, r_3 |G_{best}|^{w(t)}\ if\ rand\ < 0.5 \\ X(t+1) = G_{best} + w\, r_4 |G_{best}|^{w(t)}\ Otherwise \end{gathered} \tag{26}$$

3.2.3. Adaptive strategy

Basic PSO algorithms frequently struggle to achieve a proper balance between exploration and exploitation during the search process. This problem is especially clear in complicated situations with more than one local optimum or multi-objective function. The position update mechanism compels particles to continually move towards their previously identified optimal positions, which can limit their capacity to explore areas surrounding the known best solutions [32]. The adaptive approach to position updates can greatly improve the efficiency of an algorithm search process. This method works by dynamically refining the search space to identify the most promising solutions, using a flexible position update strategy that adjusts during each iteration. These advancements have demonstrated a significant boost in search performance [33]. A dynamic strategy for updating particle positions is introduced, focusing on either global exploration or local exploitation. The parameter p is iteratively adjusted in response to fluctuations in the fitness value, which is the primary component of this strategy. This approach effectively manages the balance between exploring new opportunities and capitalizing on established optimal solutions [23]. The expression of factor p_i is given below:

$$p_i = \frac{exp\ (fi_{COF}(X_i(t)))}{exp\ (\frac{1}{N}\sum_{i=1}^{N}(fi_{COF}(X_i(t))))} \tag{27}$$

Where N represents the total number of particles or individuals in the population. The fitness of the corresponding particle, as evaluated by the COF, is denoted as $fi_{COF}()$. The ratio p_i is a measure that depends on the adaptive position update strategy, which dynamically adjusts the balance between local

exploitation and global exploration [23]. The formula for updating position is articulated by the following relationship:

$$X_i(t+1) = w(t)\, X_i(t) + \big(1 - w(t)\big)\, V_i(t+1) + G_{best}(t)\ if\ p_i\ > rand$$
$$XX_i(t+1) = X_i(t) + \ V_i(t+1)\ Otherwise \quad (28)$$

In each iteration, a ratio p_i is computed by contrasting the fitness value of the current particle with the average fitness value of the population. When p_i is minimal, it signifies that the fitness value of particle i above the population average, indicating that the particle is near the optimal position and requires improvement in its local exploitation abilities. To enhance the global exploration capability of particle i, the location update approach $X = X + VX$ is employed. Conversely, a big p_i signifies that particle i occupies a poor position (indicating that particle i is performing below the average level of the population) and necessitates modifications to improve global exploration capabilities and avert premature convergence. In this context, the location update approach $X = wX + (1 - w)V$ is utilized to enhance local exploitation [23].

3.2.4. Symmetric cooperative swarms

Symmetry plays a pivotal role in algorithm design and application, simplifying complex problems and improving efficiency across various fields. For instance, the divide-and-conquer method utilizes symmetry to reduce search space and time complexity, while in image processing, symmetrical properties of objects optimize rendering and computational overhead. Similarly, database optimization benefits from symmetry through techniques like normalization and indexing, which eliminate redundancies and accelerate data queries.

In particle swarm optimization, exploration and exploitation are balanced through a two-group strategy. The elite group employs advanced techniques, such as velocity pausing and adaptive adjustments, to refine exploration and exploitation within local spaces. Conversely, the non-elite group focuses on global best references to promote diverse and extensive exploration. This cooperative framework enhances the algorithm's ability to identify optimal solutions efficiently and effectively [23].

3.2.5. Last-place elimination mechanism

The terminal replacement mechanism, often referred to as the “last-place elimination mechanism” is a common algorithmic approach inspired by natural selection principles, such as survival of the fittest. Widely applied in optimization and genetic algorithms, it facilitates the identification of optimal solutions under resource constraints or competitive conditions. The process involves generating and ranking candidate solutions based on specific criteria. Low-ranking candidates are iteratively removed, while higher-ranking one’s progress through further evaluations until the optimal solution is found or a stopping condition is met.

To enhance adaptability and mimic real-world uncertainties, the particle swarm optimization (PSO) algorithm incorporates an elimination factor. This probabilistic element allows selective replacement of particles based on predetermined rules, improving the algorithm robustness and flexibility, and with the integrating of this elimination factor, the algorithm not only replicates the inherent uncertainties of real-life situations but also significantly enhances its adaptability and robustness [23].

$$Gw_p(t) = argmax(fi_{COF}\left(P_{best_1}(t)\right), \ldots\ldots, fi_{COF}\left(P_{best_N}(t)\right)) \quad (29)$$

$Gw_p(t)$ “the worst particle” is the particle with the lowest $fi_{COF}()$ value among all individual ideal particles and will be replaced in each iteration, and defined as in the Eq. (29).

$$N_{best}(t) = G_{best}(t) + r_5\left(P_{best_{(h)}}(t) - P_{best_{(o)}}(t)\right) \quad h \neq o \ \in (1,2 \dots \dots, N) \tag{30}$$

N_{best} is computed through the intersection between the swarm's global best particle and with two distinct individual best particles, $P_{best(h)}$ and $P_{best(o)}$. Here, $r_5 \in [0, 1]$ is a random number in Eq. (30). The substitution mechanism is defined as,

$$Gw_p(t) = N_{best}(t) \quad if\ fi_{COF}(N_{best}(t)) < fi_{COF}(Gw_p(t))$$
$$Gw_p(t) = Gw_p(t) \quad Otherwise \tag{31}$$

The fitness values of the newly generated particle N_{best} and the less optimal particle $Gw_p(t)$ are compared. If N_{best} shows superior fitness, it replaces $Gw_p(t)$, otherwise $Gw_p(t)$ is retained and the eliminated particle is chosen accordingly.

As illustrated in Fig. 1, the optimization process is comprised of multiple distinct steps. The following flowchart delineates the primary steps to be taken in order to achieve optimal results through the utilization of the VAS-PSO algorithm.

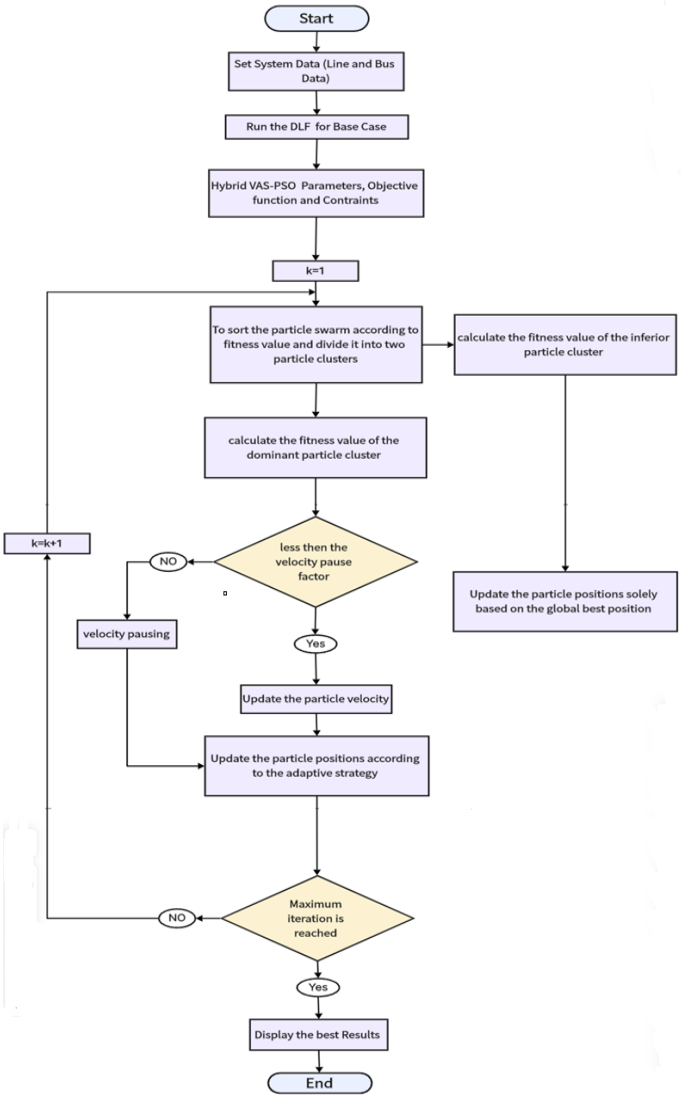

Figure 1. The proposed flowchart of VAS-PSO algorithm.

4. RESULTS AND DISCUSSION

The VAS-PSO method was implemented in the MATLAB program R2016a using a personal computer equipped with an Intel® Core i5-1035G1 CPU functioning at 1.19 GHz with 12 GB of RAM. To evaluate the integration of simultaneous PV-DGs and DSTATCOMs of varying sizes, two IEEE standard RDSs were used. The initial test system is the conventional IEEE 33 bus, seen in Fig. 2(a). The system consists of 33 buses and 32 segments, with determined active power loss and reactive power loss of 210.987 kW and 143.128 kVar, respectively. The lowest voltage is recorded at bus 18, with V_{min} = 0.9038 (p.u). The second test system, illustrated in Fig. 2(b), is the conventional IEEE 69-bus system, consisting of 69 buses and 68 branches. The value of *TAPL* and total reactive power loss (*TRPL*) in this particular system are 224.94 kW and 102.140 kVar, respectively, with V_{min} = 0.9092(p.u). Comprehensive information regarding these standard test systems is available in References [34,35]. Furthermore, Tables 1 and 2 offer an exhaustive delineation of the two RDS test systems, including their limit values. The tuned parameters of VAS-PSO algorithm are listed in Table 3.

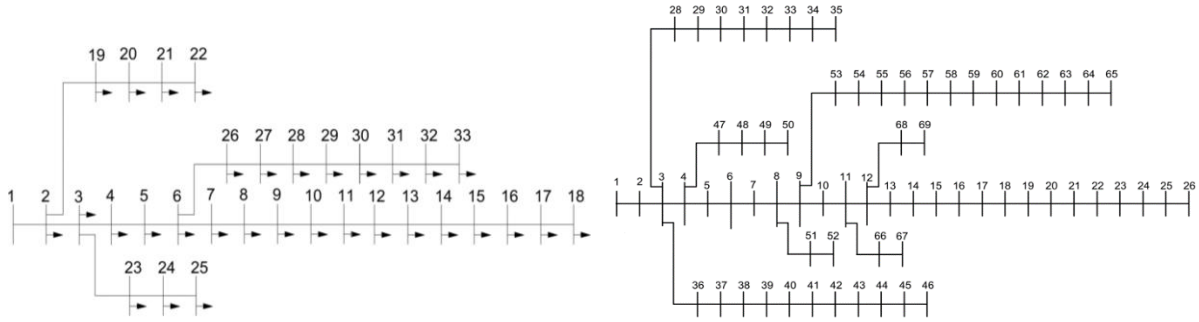

(a) *(b)*

Figure 2. Standard RDS single line diagrams: (a) IEEE 33 bus and (b) IEEE 69 bus.

Table 1. Limit values for test system constraints.

Constraints	Limits	IEEE 33-bus	IEEE 69-bus
Number of PVDGs		3	3
P_{PVDG} (kW)	Min	20	20
	Max	3000	3000
Number of DSTATCOMs		3	3
$Q_{DSTATCOM}$ (kVar)	Min	0	0
	Max	2000	2000
V_{bus}(p.u)	Min	0.95	0.95
	Max	1.05	1.05
ΔV_{max} (%)		5	5

Table 2. Description of test systems.

Description	IEEE-33 Bus	IEEE-69 Bus
Number of buses	33	69
Number of branches	32	68
base voltage (KV)	12.66	12.66
V_{min}(p.u)	0.9038	0.9092
VSI_{min}(p.u)	0.661	0.6822
P_{loss}(kW)	210.98	224.94
TVD(p.u)	1.812	1.870

Table 3. Adjusted parameters of the proposed algorithm.

Algorithm	Parameter	Description	Value
VAS-PSO	maxitr	Description: Maximum number of iterations	300
	N_{pop}	Swarm size	30
	C_1	Cognitive acceleration coefficients	2
	C_2	Social acceleration coefficients	2
	N_{runs}	Number of runs	50
	b	constant value	2
	a	velocity pausing parameter	[0,1]

To examine the effectiveness of the suggested algorithms, four distinct situations are examined for the two RDS, as illustrated below:

Case 1: Without integration.
Case 2: PV-DG Integration only.
Case 3: DSTATCOM Integration only.
Case 4: PV-DG and DSTATCOM simultaneous integration.
Case 5: PV-DG and DSTATCOM simultaneous integration with peak load (1.2).

The VAS-PSO algorithm demonstrated satisfactory performance in terms of efficiency and reliability, leading to a significant reduction in COF, where it outperformed both the m-HMO and FA-SCAS-PSO algorithms in achieving the best reduction in TAPL for both RDS systems.

Figs. 3(a,b) display the convergence curve for the suggested method when applied to the IEEE 33 and 69 bus test systems for PV-DG integration only. We observe that the VAS-PSO algorithm converges to the minimum *COF* (*TAPL*) value for the first test system with 33 buses after 150 iterations. For the second test system, the IEEE 69 buses, the VAS-PSO algorithm achieves the minimum TAPL value within 150 iterations.

Figs. 4(a,b) shows the convergence curve for the proposed method when used with the IEEE 33- and 69-bus test systems for DSTATCOM integration only. For the first test system with 33 buses, the VAS-PSO algorithm converges to the minimum *COF* (*TAPL*) value before 150 iterations. The minimum *TAPL* value is obtained for the second test system (IEEE 69 buses) before 200 iterations.

Figs. 5(a,b) presents the convergence curve of the proposed approach for simultaneous integration of PV-DG and DSTATCOM on the IEEE 33- and 69-bus test systems. For the 33-bus network, the VAS-PSO algorithm reaches the minimum *COF* (*TAPL*) after 200 iterations. Similarly, for the IEEE 69-bus system, the algorithm converges to achieve the minimum *TAPL* before 200 iterations.

Figs. 6(a,b) shows the convergence curve of the proposed algorithm for the simultaneous integration of PV-DG and DSTATCOM on the IEEE 33- and 69-bus test systems when the load increases by a factor of 1.2. For the first testing system, the VAS-PSO algorithm reaches the minimum *COF* (*TAPL*) before 200 iterations. For the second test system, the algorithm converges to achieve the minimum *TAPL* within 150 iterations.

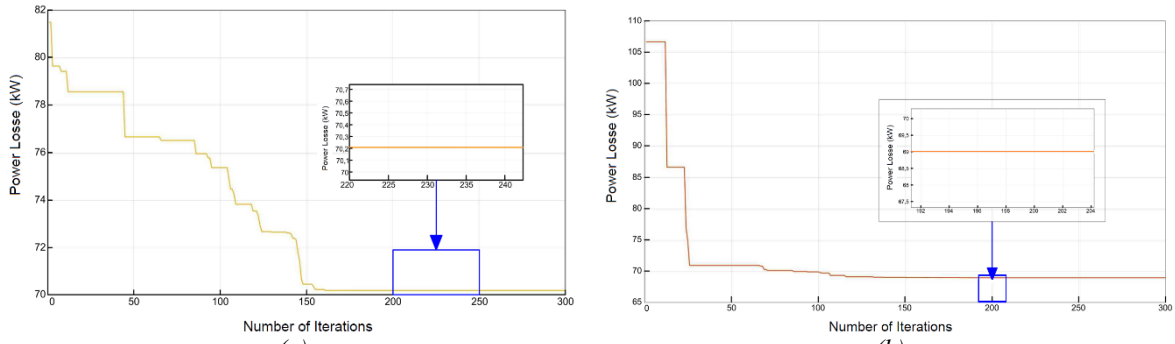

(a) *(b)*

Figure 3. Convergence curve of second cases using VAS-PSO algorithm: (a) IEEE 33-bus, (b) IEEE 69-bus.

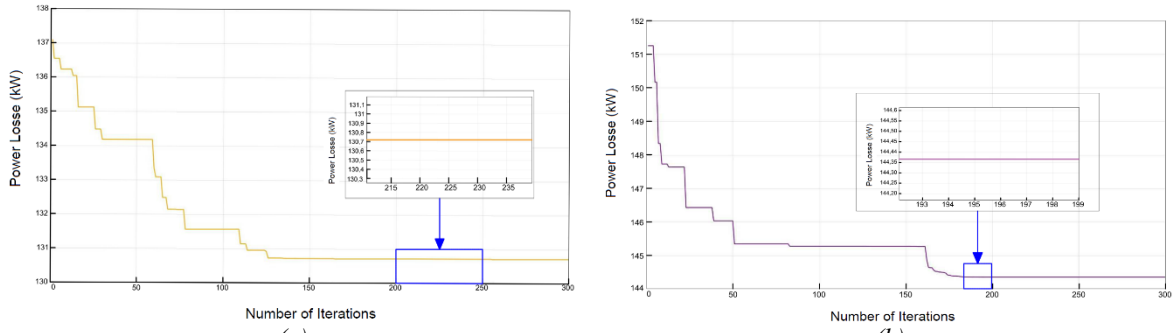

(a) (b)

Figure 4. Convergence curve of third cases using VAS-PSO algorithm: (a) IEEE 33-bus, (b) IEEE 69-bus.

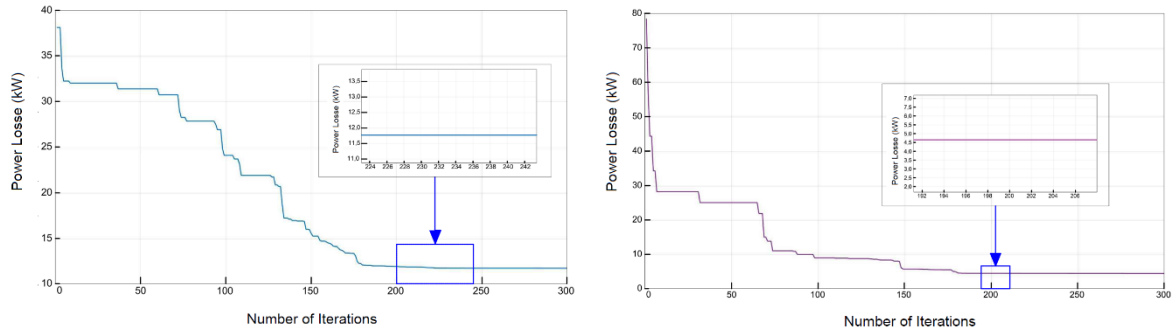

(a) (b)

Figure 5. Convergence curve of fourth case using VAS-PSO algorithm: (a) IEEE 33-bus, (b) IEEE 69-bus.

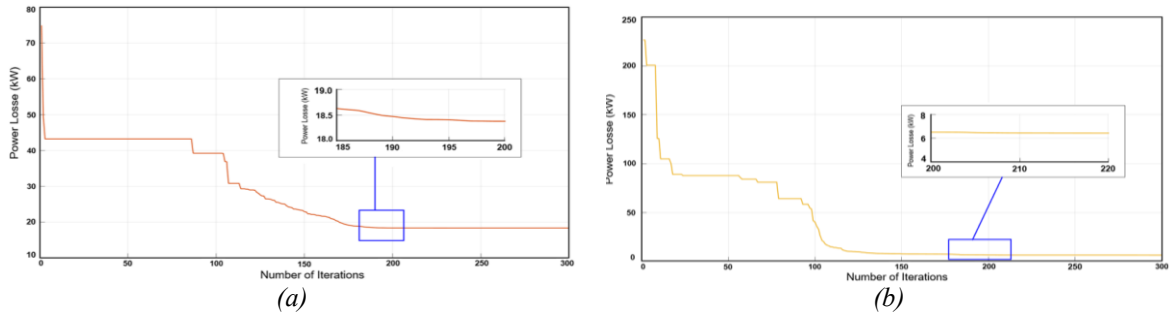

(a) (b)

Figure 6. Convergence curve of Fifth case using VAS-PSO algorithm: (a) IEEE 33-bus, (b) IEEE 69-bus.

The results presented in Tables 4 and 5 illustrate various technical values derived from the proposed VAS-PSO method following the integration of only PVDG (Case 2) for the two IEEE test systems. As shown in Table 4, when comparing the optimal results obtained for the first test system consisting of 33 buses where only PVDG is integrated (Case 2) with a set of results from other implemented algorithms, the lowest values for *TAPL* and *TVD* were achieved by VAS-PSO, which identified buses 14, 25, and 30 as ideal locations for integrating PV-DG units with sizes of 0.738 MW, 0.771 MW, and 1.092 MW, respectively for each station. The TAPL was reduced from 210.98 kW (Case 1) to 70.213 kW with a reduction rate of 66.72%, while the TRPL was reduced from 143.12 kVar to 48.33 kVar with a reduction rate of 66.23%. Meanwhile, the total voltage deviation (*TVD*) value decreased from 1.812 (p.u) in the initial case to 0.571 (p.u), with a reduction rate of 68.49%. V_{min} was improved from 0.9038 (p.u) to 0.975 (p.u). The value of the velocity pausing parameter "a" in this case, which gave the best results, was set at 0.4.

Table 5 displays the results of the second test system. It can be noted that the best value of *COF* is obtained by VAS-PSO. The results indicate the best decrease in the *TVD* achieved through the proposed VAS-PSO algorithm, compared to the results from other listed algorithms. The proposed algorithm identifies buses 12, 21, and 61 as suitable locations for integrating PVDG modules with capacities of 0.379 MW, 0.321 MW, and 1.700 MW, respectively, for each station. This integration contributed to maximizing the *TAPL* reduction ratio of 69.32%, as the *TAPL* decreased from 224.94 kW to 69.01 kW,

while the *TRPL* value decreased from 102.14 KVar to 34.99 KVar at a rate of 65.74%. As for the *TVD* value, it decreased from 1.87 (p.u) to 0.496 (p.u), i.e., an improvement rate of 73.55%. In addition, V_{min} is increased from 0.9092 (p.u) to 0.9813 (p.u). The velocity pausing parameter coefficient was set at 0.2, resulting in the optimal values for this case.

Table 4. Comparison of optimal results when PVDG is installed only (Case 2) for IEEE 33-bus.

Method	P_{loss} (kW)	ΔP_{loss} %	PVDG		TVD (p.u)	Q_{loss} (kVar)	V_{min} (p.u)
			Bus location	P_{PVDG} (MW)			
Basic PSO [1]	74.674	64.61	12	0.912	NaN	51.550	0.962
			24	1.071			
			31	0.790			
MOGOA [36]	84.85	59.78	12	0.123	NaN	NaN	0.963
			28	2.369			
			31	0.241			
FA-SCAC-PSO [1]	74.101	64.88	13	0.818	NaN	51.153	0.966
			25	0.703			
			30	1.034			
VAS-PSO	70.213	66.72	14	0.738	0.571	48.334	0.975
			25	0.771			
			30	1.092			

Table 5. Comparison of optimal results when PVDG is installed only (Case 2) for IEEE 69-bus.

Method	P_{loss} (kW)	ΔP_{loss} %	PVDG		TVD (p.u)	Q_{loss} (kVar)	V_{min} (p.u)
			Bus location	P_{PVDG} (MW)			
Basic PSO [1]	70.089	68.84	12	0.300	NaN	35.331	0.976
			22	0.383			
			61	1.694			
FA-SCAC-PSO [1]	70.135	68.82	12	0.324	NaN	35.376	0.976
			21	0.350			
			61	1.671			
CC-TVA-PSO [2]	87.35	61.17	32	0.649	1.266	NaN	NaN
			61	1.012			
			62	0.616			
VAS-PSO	69.010	69.32	12	0.379	0.496	34.992	0.981
			21	0.321			
			61	1.700			

The simulation results listed in Tables 6-7 represent the technical values obtained using the proposed hybrid VAS-PSO algorithm after integrating DSTATCOM only (Case 3) for the two RDSs. The first test system is the IEEE 33-bus. As mentioned in Table 6, the results indicate that the VAS-PSO algorithm is more efficient in terms of reducing *TAPL* and *TVD*, with buses 14, 24, and 30 identified as the best locations for integrating DSTATCOM units with capacities of 0.400 MVar, 0.514 MVar, and 1.050 MVar, respectively, for each station. In this system, the *TAPL* value decreased from 210.98 kW to 130.71 kW, achieving a maximum reduction rate of 38.04%. Moreover, the proposed algorithm achieved a substantial decrease for the *TVD* from 1.812 (p.u) to 1.115 (p.u) with an improvement rate of 38.47%, while VAS-PSO attained the optimal result for *Vmin*, obtaining a result of 0.944 (p.u). The velocity pausing coefficient was set at 0.2, resulting in the optimal values for this case.

The simulation results of the IEEE 69-bus RDS are presented in Table 7. VAS-PSO achieves the optimal value of *COF*. The findings demonstrate that the proposed VAS-PSO algorithm yields the most significant reduction in *TVD* and *TAPL* when compared to the outcomes of other methods. The proposed algorithm found that buses 11, 21, and 61 were the best locations for integrating DSTATCOM modules with optimal sizes of 0.360 MVar, 0.238 MVar, and 1.267 MVar per bus, respectively. Furthermore, the VAS-PSO algorithm achieved the lowest *TAPL* value compared to the algorithms mentioned in Table 7, which is reduced from 224.94 kW to 144.36 kW. Similarly, the VAS-PSO algorithm recorded the

best result for *TVD* at 1.378 (p.u) compared to the initial case, and it also achieved the best V_{min} value of 0.9342 (p.u). Setting the velocity pausing parameter at 0.4 yielded the optimal results for this case.

Table 6. Comparison of optimal results when DSTATCOM is installed only (Case 3) for IEEE 33-bus

Method	P_{loss} (kW)	ΔP_{loss} %	PVDG		TVD (p.u)	Q_{loss} (kVar)	V_{min} (p.u)
			Bus location	$Q_{DSTATCOM}$ (MVar)			
Basic PSO [1]	141.82	32.78	15	0.314	NaN	96.6374	0.932
			23	0.656			
			29	1.139			
MoSCA [37]	135.20	35.92	30	0.771	NaN	NaN	0.942
			4	0.993			
			11	0.425			
FA-SCAC-PSO [1]	138.39	34.41	14	0.402	NaN	94.44	0.934
			24	0.553			
			30	1.059			
VAS- PSO	130.71	38.04	14	0.400	1.115	87.42	0.944
			24	0.514			
			30	1.050			

Table 7. Comparison of optimal results when DSTATCOM is installed only (Case 3) for IEEE 69-bus

Method	P_{loss} (kW)	ΔP_{loss} %	PVDG		TVD (p.u)	Q_{loss} (kVar)	V_{min} (p.u)
			Bus location	$Q_{DSTATCOM}$ (MVar)			
Basic PSO [1]	148.62	33.93	11	0.706	NaN	68.92	0.934
			61	1.412			
			64	0.010			
FA-SCAC-PSO [1]	145.09	35.5	11	0.386	NaN	67.65	0.931
			20	0.235			
			61	1.236			
MoSCA [37]	149.1	33.72	4	1.448	NaN	NaN	0.939
			55	1.589			
			63	0.900			
VAS-PSO	144.36	35.82	11	0.360	1.37	67.50	0.934
			21	0.238			
			61	1.267			

The results obtained in Table 8 for the first test system (IEEE 33-bus system) show that the simultaneous integration of PVDG and DSTATCOM helps lower the *TAPL* to a satisfactory level. The results obtained demonstrate that the VAS-PSO algorithm outperforms the mHMO, CSOA, and FA-SCAC-PSO algorithms in obtaining the best *COF* values. It also finds buses 14, 24, and 30 as the best places to put PVDG modules, with the best sizes of 0.729 MW, 0.998 MW, and 1.026 MW injected into each bus, respectively. Furthermore, buses 13, 24, and 30 were found to be the best places to integrate DSTATCOM units, with the best sizes being 0.364 MVar, 0.516 MVar, and 1.009 MVar, as shown in Fig. 7(a). This integration reduced the *TAPL* from 210.98 kW to 11.760 kW, which is a 94.43% drop. On the other hand, the minimum *TVD* is obtained when using the proposed algorithm, which is 0.155 (p.u), with a reduction of 91.45%. The minimum voltage V_{min} is increased from 0.9038 (p.u) to 0.992 (p.u).The value of "a" in this case, which gave the best results, was determined to be 0.3.

Regarding the second test system (69 bus), as illustrated in Table 9, the VAS-PSO algorithm identifies buses 12, 19, and 61 as the optimal locations for installing PVDG modules with ideal power sizes of 0.394 MW, 0.338 MW, and 1.687 MW, respectively. Similarly, buses 11, 18, and 61 are the best locations for installing DSTATCOM modules with ideal sizes of 0.304 MVar, 0.300 MVar, and 1.198 MVar, as shown in Fig. 7(b). The optimal value of "a" for best results was determined to be 0.4. This integrated approach led to a significant reduction in *TAPL* from 224.94 kW to 4.589 kW, representing a 97.96% decrease. Furthermore, the *TVD* value with the suggested algorithm was 0.1283 (p.u). The V_{min} improved from 0.9092 (p.u) to 0.9943 (p.u).

Table 8. Comparison of optimal results with simultaneous installation of PVDG and DSTATCOM (Case 4) for IEEE 33-bus.

Method	P_{loss} (kW)	ΔP_{loss} %	PVDG		DSTATCOM		TVD (p.u)	ΔTVD %	V_{min} (p.u)
			Bus location	P_{PVDG} (MW)	Bus location	$Q_{DSTATCOM}$ (MVar)			
Basic PSO [1]	25.419	87.95	3	0.831	18	0.214	NaN	NaN	0.988
			14	0.904	25	0.375			
			30	0.971	30	1.450			
HMO [4]	13.236	93.73	10	0.904	14	0.362	0.194	89.63	NaN
			24	0.902	24	0.516			
			30	0.946	30	1.0175			
mHMO [4]	12.093	94.27	14	0.754	13	0.373	0.170	90.91	NaN
			24	0.927	24	0.514			
			30	1.006	30	1.012			
TVA-PSO [38]	22.882	89.15	13	0.771	4	0.778	NaN	NaN	0.976
			24	0.780	29	0.631			
			30	0.773	30	0.588			
FA-SCAC-PSO [1]	13.496	93.57	13	0.896	13	0.389	NaN	NaN	0.993
			25	0.652	24	0.476			
			30	1.068	30	1.058			
BFOA [18]	15.070	92.85	12	0.850	12	0.400	NaN	NaN	0.986
			25	0.750	25	0.350			
			30	0.860	30	0.850			
WCA [17]	24.880	88.20	25	0.973	23	0.465	NaN	NaN	0.980
			29	1.040	30	0.565			
			11	0.563	14	0.535			
CSOA [19]	12	94.31	14	0.750	11	0.420	NaN	NaN	0.991
			24	1.100	24	0.460			
			30	1.000	30	0.970			
BWOA [12]	25.415	87.95	10	0.806	6	0.774	NaN	NaN	0.978
			24	0.830	30	0.847			
			33	0.620	33	0.259			
VAS- PSO	11.760	94.43	14	0.729	13	0.364	0.155	91.45	0.992
			24	0.998	24	0.516			
			30	1.026	30	1.009			

Table 9. Comparison of optimal results with simultaneous installation of PVDG and DSTATCOM (Case 4) for IEEE 69-bus.

Method	P_{loss} (kW)	ΔP_{loss} %	PVDG		DSTATCOM		TVD (p.u)	ΔTVD %	V_{min} (p.u)
			Bus location	P_{PVDG} (MW)	Bus location	$Q_{DSTATCOM}$ (kVar)			
Basic PSO [1]	19.410	91.37	27	0.375	25	0.318	NaN	NaN	0.980
			60	0.741	27	0.013			
			63	0.597	61	1.211			
HMO [4]	6.621	97.06	17	0.448	12	0.541	0.191	89.79	NaN
			53	0.300	28	0.426			
			61	1.641	61	1.211			
mHMO [4]	4.788	97.87	12	0.368	18	0.354	0.145	92.25	NaN
			21	0.319	50	0.506			
			61	1.655	61	1.238			
TVA-PSO [38]	10.669	95.24	12	0.915	11	0.778	NaN	NaN	0.988
			22	0.134	24	0.094			
			61	1.361	61	1.223			
FA-SCAC-PSO [1]	5.160	97.71	17	0.355	11	0.400	NaN	NaN	0.994
			61	1.753	17	0.267			
			69	0.407	61	1.158			
CSOA [19]	8.070	96.41	17	0.490	25	0.270	NaN	NaN	0.992
			61	1.400	61	0.980			
			63	0.250	63	0.200			
WCA [17]	33.339	85.12	17	0.540	2	1.187	NaN	NaN	0.994
			61	2.000	62	1.237			
			69	1.159	69	0.269			
BWOA [12]	34.229	84.78	11	0.861	29	0.271	NaN	NaN	0.970
			61	0.878	60	0.723			
			66	0.035	69	0.014			
VAS- PSO	4.589	97.96	12	0.394	11	0.304	0.128	93.16	0.994
			19	0.338	18	0.300			
			61	1.687	61	1.198			

Fig. 7 illustrates the optimal simultaneous placement of PVDG and DSTATCOM in two RDS for the Case 4.

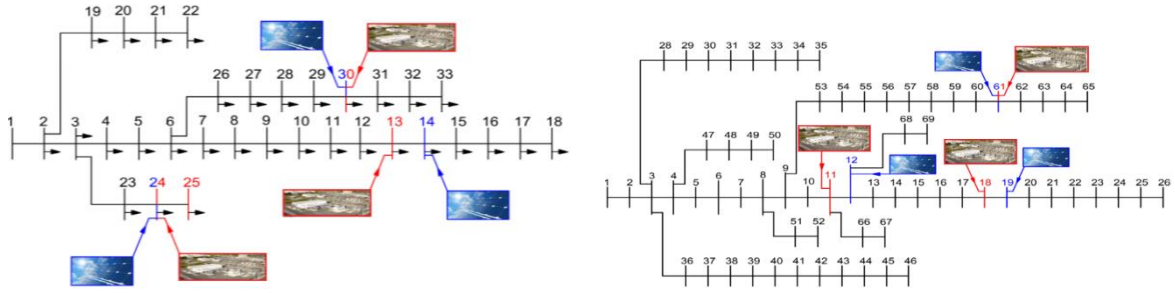

(a) *(b)*

Figure 7. Optimal PVDG and DSTATCOM locations in standard RDS: (a) IEEE.33 bus, (b) IEEE.69 bus.

Figs. 8(a,b) illustrate the bus voltage profiles for several scenarios examined in the two RDS (IEEE 33 bus and IEEE 69bus), utilizing the VAS-PSO algorithm. This figure shows the effect of implementing PVDG and DSTATCOM at the same time on the voltage profile of each system. For the IEEE 33 and 69 bus, it demonstrates that the voltage profile enhances across all three case studies (integration of PVDG only, integration of DSTATCOM only, and simultaneous integration of PVDG and DSTATCOM) in comparison to the base scenario. The simultaneous integration of PVDG and DSTATCOM yields the most significant improvement to the voltage profile.

The minimum voltage increases from 0.9038 (p.u) to 0.992(p.u) in the first test system as shown in Fig. 8(a), and from 0.9092 (p.u) to 0.9943(p.u) in the second test system as shown in Fig. 8(b) with the concurrent presence of PVDG and DSTATCOM.

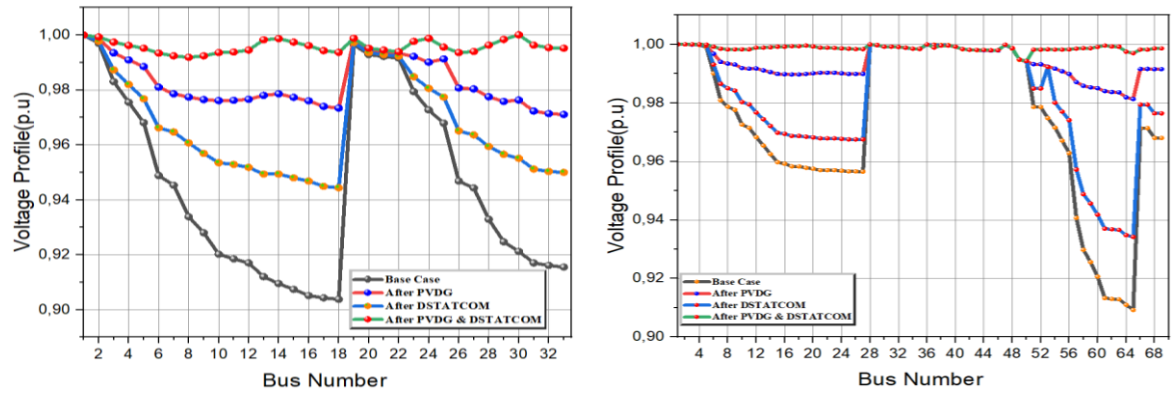

(a) *(b)*

Figure 8. Bus voltage profiles for different case studies: (a) IEEE 33-bus, (b) IEEE 69-bus.

Fig. 9 details the impact of integrating PVDG and DSTATCOM on power losses within each branch of the two tested radial distribution systems (RDS). The study examines the effects of integrating PVDG only, DSTATCOM only, and integrating PVDG and DSTATCOM simultaneously. The analysis reveals that the simultaneous integration of PVDG and DSTATCOM achieves the greatest reduction in *TAPL* across all branches, exceeding the improvements seen with PVDG or DSTATCOM alone.

This approach reduces the maximum power loss in the branches of the IEEE 33 bus from 52.097 kW to only 1.3547 kW, as illustrated in Fig. 9(a). For the IEEE 69-bus RDS, this approach reduces the maximum power loss in the different branches from 49.67 kW to just 1.22 kW, as illustrated in Fig. 9(b).

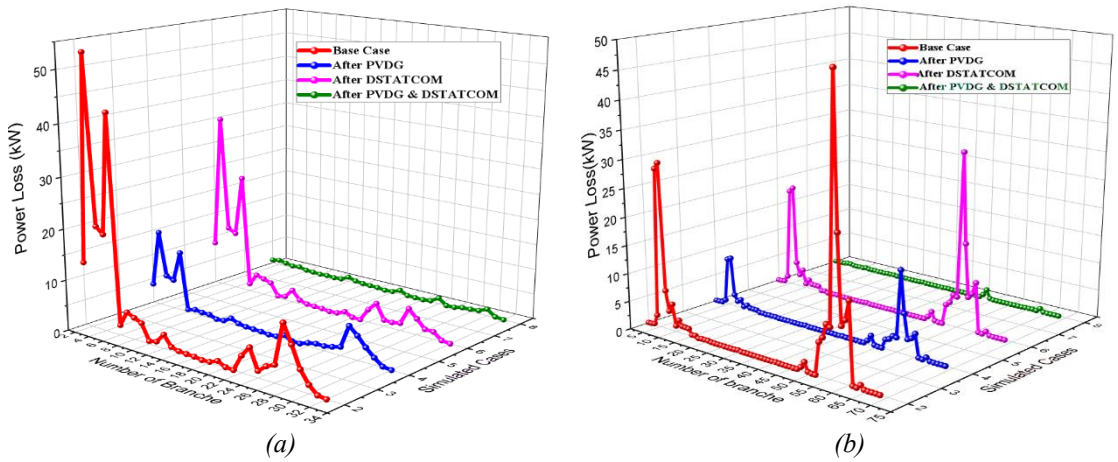

(a) (b)

Figure 9. Active power loss in branch lines for different case studies: (a) IEEE 33-bus, (b) IEEE 69-bus.

Fig. 10 shows the comparison of *TAPL* results in the two RDS for different cases. Here we see the effect of integrating both PVDG and DSATCOM simultaneously in the two RDS on reducing total power losses compared to the other cases.

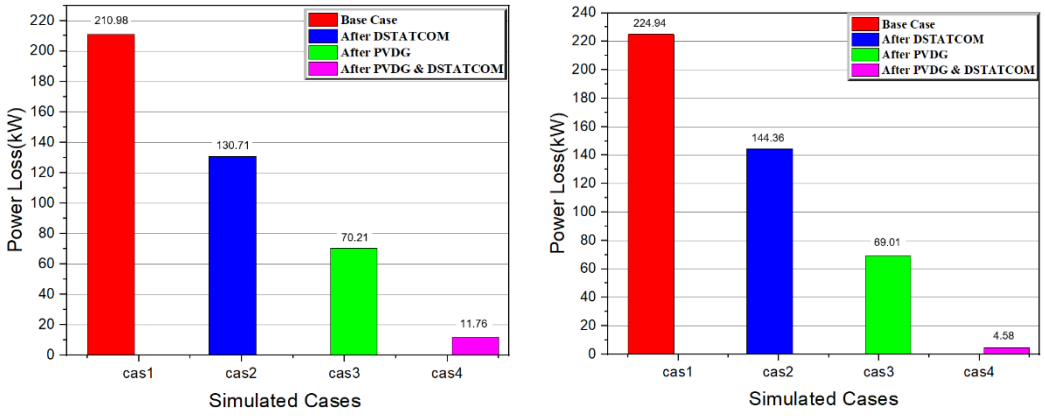

(a) (b)

Figure 10. Total active power losses of RDS for different cases: (a) IEEE 33-bus, (b) IEEE 69-bus.

Fig. 11 compares the *TAPL* results obtained using the proposed algorithm with those obtained using other algorithms. It can be definitively concluded that the proposed algorithm resulted in lower *TAPL* for both test systems: A *TAPL* value of 11.76 kW for the first test system and 4.58 kW for the second test system. These values are lower than the mHMO values of 12.093 kW and 4.78 kW, respectively, for the two systems.

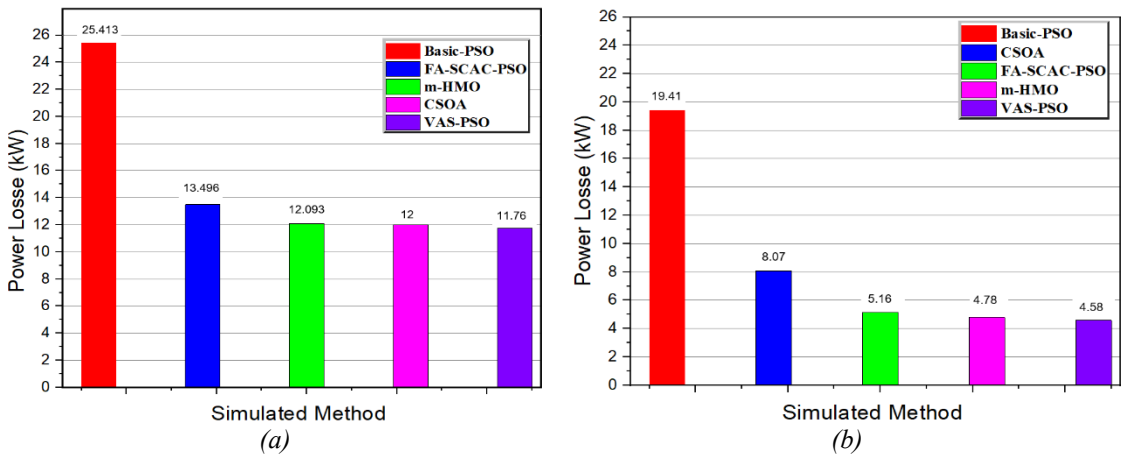

(a) (b)

Figure 11. Comparison of the results of different algorithms regarding TAPL: (a) IEEE 33-bus, (b) IEEE 69-bus

Fig. 12 presents a comparison of V_{min}, VSI_{min}, and *TVD* across the four situations for both RDS systems. Analysis of various case studies within the two test systems demonstrates that the simultaneous integration of PVDG and DSTATCOM produces excellent results for the three indicators, with the V_{min} and VSI_{min} ratios achieving approximately 9.76% and 46.17%, respectively, while the *TVD* was diminished by 91.45% for the first test system. The V_{min} and VSI_{min} ratios were optimized to roughly 9.36% and 43.13%, respectively, while the TVDI was decreased by 93.14% for the second test system (69-bus). Table 10 illustrate the variations in the *VSI* for each scenario between the first and the second test systems. Table 11 summarizes the statistical results found in the tests for Cases 2,3, and 4.

Table 10. The comparison of the minimal voltage stability index for several scenarios.

VSI_{min} (p.u)	Case 1	Case 2	Case 3	Case 4
IEEE 33 bus	0.661	0.889	0.7952	0.9662
IEEE 69 bus	0.682	0.927	0.760	0.9766

Table 11. Statistical assessment for the proposed algorithm for Cases 2-4 for two RDS.

Cases studies	Parameters	Case2	Case 3	Case 4
IEEE 33 bus	Mean	70.82	131.46	14.71
	Best	70.21	130.71	11.76
	Rank	2	3	1
IEEE 69 bus	Mean	69.4422	144.59	6.74
	Best	69.01	144.36	4.589
	Rank	2	3	1

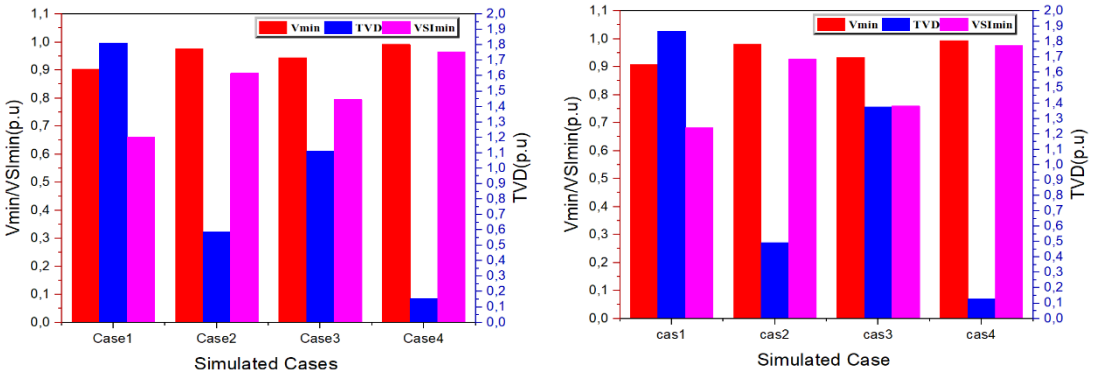

(a) *(b)*

Figure 12. Minimum voltage and total voltage deviation with minimum voltage stability index of RDS for different cases: (a) IEEE 33-bus, (b) IEEE 69-bus.

Figs. 13(a,b) and Figs. 14(a,b) present the results for the *TAPL* in both systems. The variation in *TAPL* is seen for the IEEE 33-bus system after each run between 11.76 kW and 20.59 kW, where the best value of *TAPL* is found for run number 29. In the same context, the *TAPL* for the IEEE 69-bus system vary between 4.58 kW and 10.66 kW, of course if we take the value of 44.7 kW as an anomaly. Figs. 15(a,b) present the results for the *TAPL* in each execution for both systems.

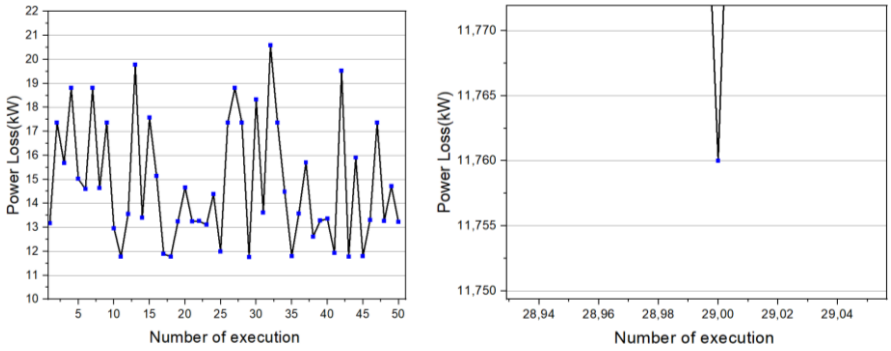

(a) *(b)*

Figure 13. (a) Total active power loss and (b) minimum power loss curves varying with number of execution for the case 4 of RDS under IEEE 33-bus.

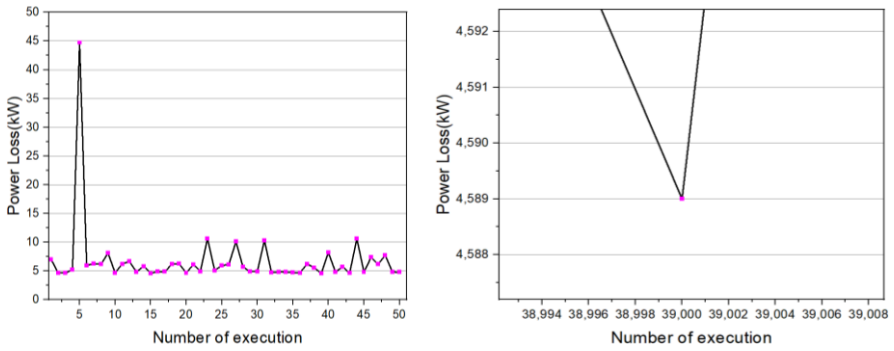

(a) (b)

Figure 14. (a) Total active power loss and (b) minimum power loss curves varying with number of execution for the case 4 of RDS under IEEE 69-bus.

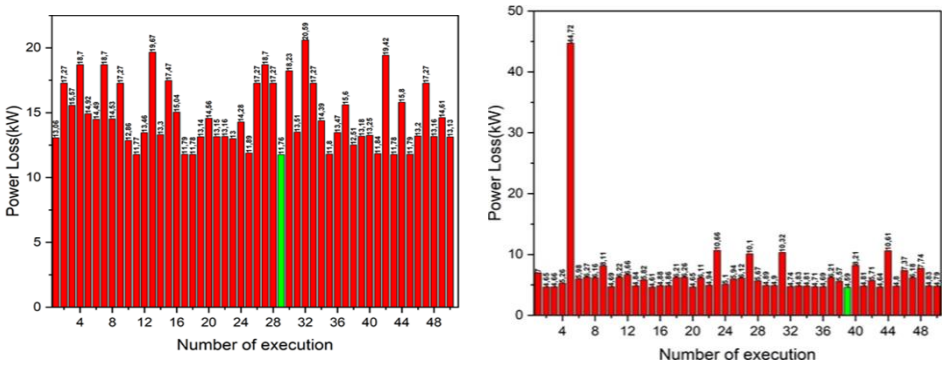

(a) (b)

Figure 15. Total active power loss curves varying with number of execution for the case 4 of RDS: (a) IEEE 33-bus, (b) IEEE 69-bus.

The results in Table 12 for the first test system (IEEE 33-bus system) show that the simultaneous integration of PVDG and DSTATCOM reduces the *TAPL* to a satisfactory level during peak load. It also determines that buses 14, 24, and 30 are the optimum places to install PVDG modules, with optimal sizes of 0.848 MW, 1.079 MW, and 1.273 MW injected into each bus, respectively.

Table 12. Optimal results of simultaneous integration of PVDG & DSTATCOM with peak load in IEEE 33-bus

Cases	P_{loss} (kW)	ΔP_{loss} %	PVDG		DSTATCOM		TVD (p.u)	VSI_{min} (p.u)	V_{min} (p.u)
			Bus location	P_{PVDG} (kW)	Bus location	$Q_{DSTATCOM}$ (MVar)			
with increase peak load	305.66	44.88	NaN	NaN	NaN	NaN	2.095	0.6355	0.892
			NaN	NaN	NaN	NaN			
			NaN	NaN	NaN	NaN			
with peak load and PVDG & DSTATCOM	18.360	91.3	14	0.848	13	0.443	0.236	0.950	0.987
			24	1.079	25	0.474			
			30	1.273	30	1.083			

In the second test system (69 bus) as shown in Table 13, the VAS-PSO algorithm selects busses 12, 19, and 61 as the best places for placing PVDG modules with optimum power sizes of 0.652 MW, 0.411 MW, and 2.009 MW, respectively. Similarly, buses 11, 18, and 61 are suitable sites for placing DSTATCOM modules with optimal sizes of 0.301 MVar, 0.297 MVar, and 1.402 MVar. The optimal value of α for best results was discovered as 0.4.

Table 13. Optimal results of simultaneous integration of PVDG & DSTATCOM with peak load in IEEE 69-bus

Cases	P_{loss} (kW)	ΔP_{loss} %	PVDG		DSTATCOM		TVD (p.u)	VSI_{min} (p.u)	V_{min} (p.u)
			Bus location	P_{PVDG} (kW)	Bus location	$Q_{DSTATCOM}$ (MVar)			
With increase peak load	335.61	49.2	NaN	NaN	NaN	NaN	2.226	0.629	0.890
			NaN	NaN	NaN	NaN			
			NaN	NaN	NaN	NaN			
with peak load and PVDG&DSTATCOM	6.458	97.13	12	0.652	11	0.301	0.134	0.971	0.993
			19	0.411	18	0.297			
			61	2.009	61	1.402			

Figs. 16(a,b) illustrate the voltage profiles during load variation for the IEEE 33 and 69 systems. The permissible voltage thresholds for the evaluated IEEE systems are 0.95 p.u. and 1.05 p.u. for the lower and upper limits, respectively. With the peak load established at 1.2, and in the IEEE 33 bus system, the voltage profiles surpassed the permissible limits for the majority of buses, especially for buses 6–18 and 26–33, where the lowest value reached 0.892 (p.u). Subsequent to the concurrent integration of PVDG and DSTATCOM, the voltage profiles were optimized and maintained within the allowable limits for the load levels, where the lowest value reached 0.987 (p.u) as depicted in Fig. 16(a). Under the IEEE 69 bus system, the voltage profiles fell below 0.95 (p.u) between buses 15–27 and 55–66. Subsequent to the concurrent installation of PVDG and DSTATCOM, the voltages are surpassed 0.95 (p.u) as shown in Fig. 16(b). Furthermore, buses 13, 24, and 30 were shown to be the optimum sites to integrate DSTATCOM units, with optimal sizes of 0.443 MVar, 0.474 MVar, and 1.083 MVar as shown in Fig. 16(a). This integration lowered the *TAPL* from 210.98 kW to 18.36 kW, a 91.3% reduction. The proposed technique, on the other hand, yields the minimal *TVD* of 0.2363 (p.u.), representing an 86.96% reduction. The lowest voltage, V_{min}, is increased from 0.9038 (p.u.) to 0.987 (p.u.). The optimal value for a in this example was found to be 0.2.

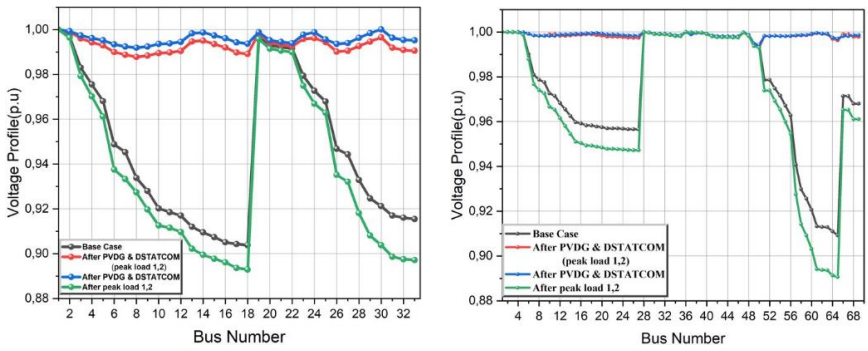

(a) *(b)*

Figure 16. Bus voltage profiles for different case studies: (a) IEEE 33-bus, (b) IEEE 69-bus

Figs. 17(a,b) show the effect of integrating PVDG and DSTATCOM on total energy losses in each branch of the two tested radial distribution systems (RDSs) at maximum load, compared with Case 4.

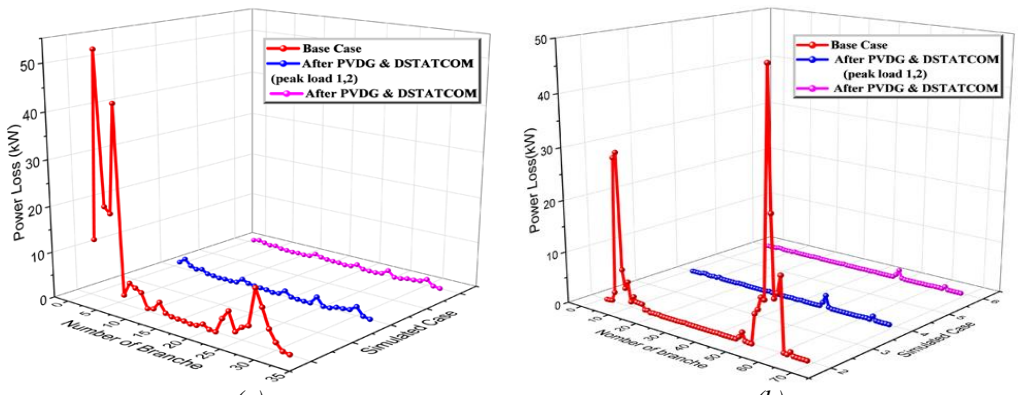

(a) *(b)*

Figure 17. Active power loss in branch lines for different case studies: (a) IEEE 33-bus, (b) IEEE 69-bus.

Figs. 18(a,b) shows a comparison of the *TAPL* results for the five cases in the two RDS systems. Here, we can see the effect that integrating both PVDG and DSATCOM simultaneously has on reducing total energy losses under increased loads in the two RDS systems. This integrated strategy resulted in a large reduction in *TAPL* from 224.94 kW to 6.458 kW, or a 97.13% decrease, as illustrated in Fig. 18(b). Furthermore, the *TVD* value using the provided algorithm was 0.134 (p.u). The V_{min} increased from 0.9092 to 0.993 (p.u).

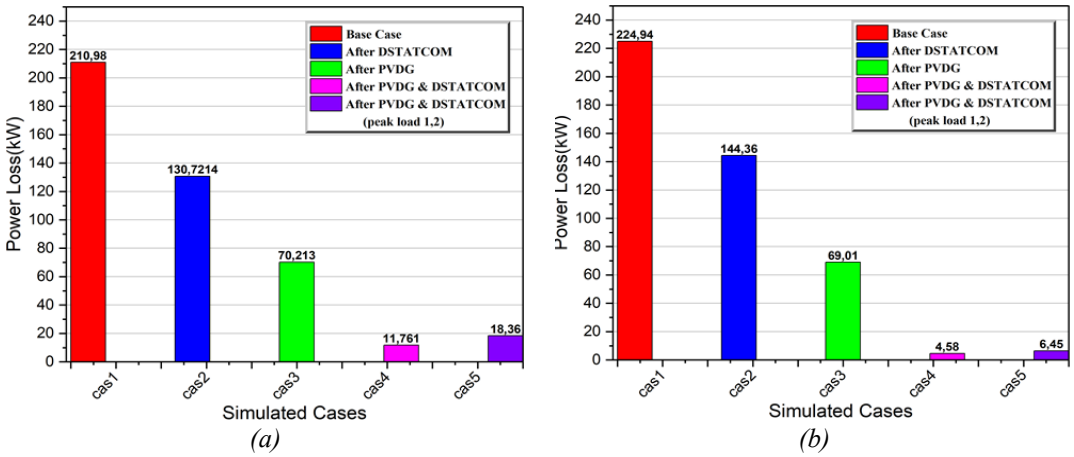

Figure 18. Total active power losses of RDS for different cases in RDS: (a) IEEE 33-bus, (b) IEEE 69-bus.

Fig. 19 shows the boxplots of *TAPL* for each execution in various cases, with VAS-PSO algorithms applied to the two test systems. As seen from the plots, the power losses vary between certain values for 2 bus systems, thus one should keep in mind to adjust the optimized result for a better solution to the network.

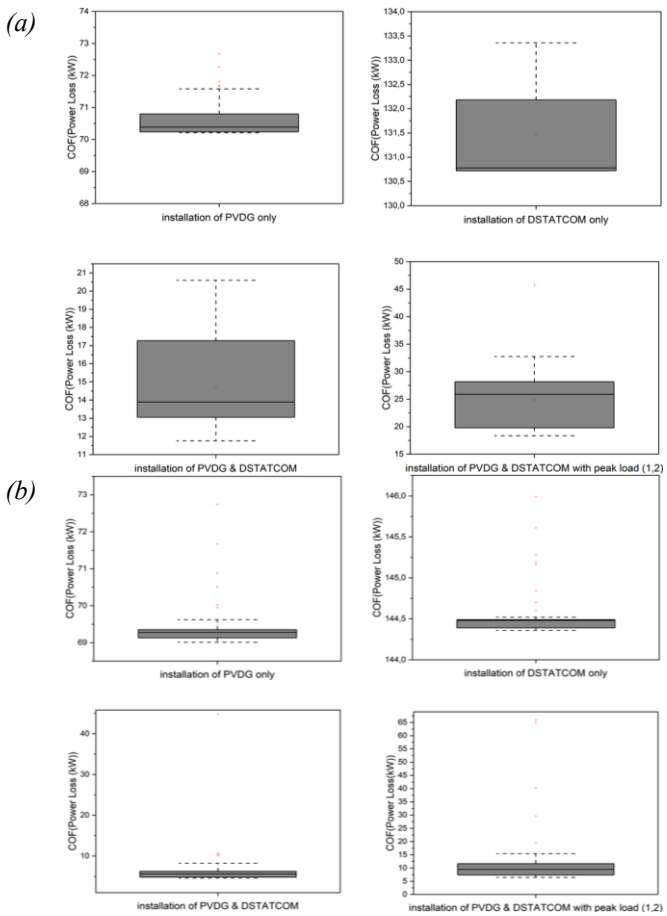

Figure 19. Boxplots of TAPL for various cases using using VAS-PSO: (a) IEEE 33-bus, (b) IEEE 69-bus

5. CONCLUSION

This work employs particle swarm optimization with velocity pausing and an adaptive strategy to optimally position and size PVDGs and DSTATCOMs in various scenarios within RDS. This reduces the *TAPL* and *TVD*, while improving the voltage profile and *VSI* values in the two standard test systems. According to the simulation data, the efficiencies of the RDSs are significantly enhanced for all investigated scenarios, particularly when the PVDGs and DSTATCOMs are connected synchronously, resulting in a decrease in *TVD* and *TAPL*. For example, the first test system (33 buses) achieved a *TAPL* reduction of up to 94.43%, while the second test system (69 buses) demonstrated a reduction of up to 97.96%. The suggested algorithm was found to be reliable and efficient in providing the best *COF* optimization outcomes compared to other well-known optimization procedures. This algorithm demonstrated a precise balance between exploitation and exploration. This is based on the use of TVIC, cooperative swarm principles, and adaptive strategies.

Future research will focus on determining the optimal deployment of distributed generators to improve the system's technical and financial metrics while considering the energy output of these generators and variations in load demand throughout the day. Several strategic approaches to improving the performance of the VAS-PSO algorithm are currently being developed, including a multi-objective VAS-PSO system that optimizes technical performance, as well as the economic and ecological benefits of integrating renewable energy with DSTATCOM. This would lead to improved operation of electrical distribution systems.

The performance of the algorithm could be improved by including time-varying acceleration coefficients in the VAS-PSO. The effectiveness of VAS-PSO can be improved through combining it with contemporary algorithms such as GWO and WOA alongside HMO.

REFERENCES

[1] Zellagui M, Lasmari A, Settoul S, El-Sehiemy RA, El-Bayeh CZ, Chenni R. Simultaneous allocation of photovoltaic DG and DSTATCOM for techno-economic and environmental benefits in electrical distribution systems at different loading conditions using novel hybrid optimization algorithms. *Int Trans Electr Energy Syst*. 2021;31:e12992. doi:10.1002/2050-7038.12992

[2] Belbachir N, Zellagui M, Lasmari A, El-Bayeh CZ, Bekkouche B. Optimal integration of photovoltaic distributed generation in electrical distribution network using hybrid modified PSO algorithms. *Indones J Electr Eng Comput Sci*. 2021;24(1):50–60. doi:10.11591/ijeecs.v24.i1.pp50-60

[3] Sujatha BC, Usha A, Geetha RS. Dynamic fuzzy learning based hybrid GWO-CSA for optimal planning of PV, BESS and DSTATCOM with network reconfiguration. *Discover Appl Sci*. 2024;6:59. doi:10.1007/s42452-024-05684-w

[4] Belbachir N, Kamel S, Hashim FA, Yu J, Zeinoddini-Meymand H, Sabbeh SF. Optimizing the hybrid PVDG and DSTATCOM integration in electrical distribution systems based on a modified homonuclear molecules optimization algorithm. *IET Renew Power Gener*. 2023;17:3075–3096. doi:10.1049/rpg2.12826

[5] Dal AR, Nasraldeen HN, Şahin HM. Efficiency analysis of fixed and axis tracking options of photovoltaic systems to be installed in a marina. *J Energy Syst*. 2024;8(1):40–52. doi:10.30521/jes.1345912

[6] Dang X, Shu X, Li F. Dynamic graph attention meets multi-scale temporal memory: a hybrid framework for photovoltaic power forecasting under high renewable penetration. *Processes*. 2025;13:873. doi:10.3390/pr13030873

[7] Ghatak SR, Sannigrahi S, Acharjee P. Optimized planning of power distribution network with solar energy, battery storage and DSTATCOM: a multi-objective approach. In: *Proceedings of the 2018 IEEE International Conference on Power Electronics, Drives and Energy Systems (PEDES)*; 2018 Dec 18–21; Chennai, India. IEEE; 2018. p. 1–6.

[8] Serdari E, Burza U. The bus selection based on PV curve for the photovoltaic integration into power grid. *J Energy Syst*. 2024;8(3):143–152. doi:10.30521/jes.1258349

[9] Kanwar N, Gupta N, Niazi KR, Swarnkar A. Improved cat swarm optimization for simultaneous allocation of DSTATCOM and DGs in distribution systems. *J Renew Energy*. 2015;2015:189080. doi:10.1155/2015/189080

[10] Rukmani DK, Thangaraj Y, Subramaniam U, Ramachandran S, Elavarasan RM, Das N, et al. A new approach to optimal location and sizing of DSTATCOM in radial distribution networks using bio-inspired cuckoo search algorithm. *Energies*. 2020;13:4615. doi:10.3390/en13184615
[11] Isha G, Jagatheeswari P. Optimal allocation of DSTATCOM and PV array in distribution system employing fuzzy-lightning search algorithm. *Automatika*. 2021;62(3):339–352. doi:10.1080/00051144.2021.1963080
[12] Shaikh R, Stojcevski A, Seyedmahmoudian M, Chandran J. A multi-objective approach for optimal sizing and placement of distributed generators and distribution static compensators in a distribution network using the black widow optimization algorithm. *Sustainability*. 2024;16:4577. doi:10.3390/su16114577
[13] Luis FG, Daniel SV, Oscar DM. Optimal integration of PV generators and D-STATCOMs into the electrical distribution system to reduce the annual investment and operational cost: a multiverse optimization algorithm and matrix power flow approach. *e-Prime Adv Electr Eng Electron Energy*. 2024;9:100747. doi:10.1016/j.prime.2024.100747
[14] Pragya G, Nitin M, Sheila M. Probabilistic distribution system planning: integrating PV-based DG, DSTATCOM, and reconfiguration under solar irradiance and load uncertainties. *Facta Univ Ser Electron Energ*. 2025;38(3):397–430. doi:10.2298/FUEE2503397G
[15] Yuvaraj T, Devabalaji KR, Thanikanti SB. Simultaneous allocation of DG and DSTATCOM using whale optimization algorithm. *Iran J Sci Technol Trans Electr Eng*. 2020;44:879–896. doi:10.1007/s40998-019-00272-w
[16] Mohammedi RD, Kouzou A, Mosbah M, Souli A, Rodriguez J, Abdelrahem M. Allocation and sizing of DSTATCOM with renewable energy systems and load uncertainty using enhanced gray wolf optimization. *Appl Sci*. 2024;14(2):556. doi:10.3390/app14020556
[17] Abou El-Ela AA, El-Sehiemy RA, Abbas AS. Optimal placement and sizing of distributed generation and capacitor banks in distribution systems using water cycle algorithm. *IEEE Syst J*. 2018;12:3629–3636.
[18] Devabalaji KR, Ravi K. Optimal size and siting of multiple DG and DSTATCOM in radial distribution system using bacterial foraging optimization algorithm. *Ain Shams Eng J*. 2016;7:959–971. doi:10.1016/j.asej.2015.07.002
[19] Yuvaraj T, Ravi K, Devabalaji KR. Optimal allocation of DG and DSTATCOM in radial distribution system using cuckoo search optimization algorithm. *Model Simul Eng*. 2017;2017:2857926. doi:10.1155/2017/2857926
[20] Isha G, Jagatheeswari P, Jasmine Gnana Malar A. Elitist Harris Hawks optimized voltage stability enhancement in radial distribution system. *J Electr Eng Technol*. 2023;18:2683–2693. doi:10.1007/s42835-023-01375-5
[21] Ferminus RA, Gnana SA. An optimization approach for optimal location and size of DSTATCOM and DG. *Appl Energy*. 2023;336:120797. doi:10.1016/j.apenergy.2023.120797
[22] Ansari A, Byalihal SC. Application of hybrid TLBO-PSO algorithm for allocation of distributed generation and STATCOM. *Indones J Electr Eng Comput Sci*. 2022;29(1):38–48. doi:10.11591/ijeecs.v29.i1.pp38-48
[23] Tang K, Meng C. Particle swarm optimization algorithm using velocity pausing and adaptive strategy. *Symmetry*. 2024;16(6):661. doi:10.3390/sym16060661
[24] Ramadan A, Ebeed M, Kamel S, Ahmed EM, Tostado-Véliz M. Optimal allocation of renewable DGs using artificial hummingbird algorithm under uncertainty conditions. *Ain Shams Eng J*. 2023;14:101872. doi:10.1016/j.asej.2022.101872
[25] Hasan EO, Hatata AY, Badran EA, et al. Optimal coordination of voltage control devices in distribution systems connected to distributed generations. *Electr Eng*. 2019;101:175–187. doi:10.1007/s00202-019-00764-2
[26] Settoul S, Chenni R, Hassan HA, Zellagui M, Kraimia MN. MFO algorithm for optimal location and sizing of multiple photovoltaic distributed generation units for loss reduction in distribution systems. In: *Proceedings of the 7th International Renewable and Sustainable Energy Conference (IRSEC)*; 2019 Nov 27–30; Agadir, Morocco. IEEE; 2019. p. 1–6.
[27] Kellogg WD, Nehrir MH, Venkataramanan G, Gerez V. Generation unit sizing and cost analysis for stand-alone wind, photovoltaic, and hybrid wind/PV systems. *IEEE Trans Energy Convers*. 1998;13:70–75. doi:10.1109/60.658206
[28] Settoul S, Zellagui M, Abdelaziz AY, Chenni R. Optimal integration of renewable distributed generation in practical distribution grids based on moth-flame optimization algorithm. In: *Proceedings of the International Conference on Advanced Electrical Engineering (ICAEE)*; 2019 Nov 19–21; Algiers, Algeria. IEEE; 2019. p. 1–5.
[29] Hassan HA, Zellagui M. MVO algorithm for optimal simultaneous integration of DG and DSTATCOM in standard radial distribution systems based on technical-economic indices. In: *Proceedings of the 21st International Middle East Power Systems Conference (MEPCON)*; 2019 Dec 17–19; Cairo, Egypt. IEEE; 2019. p. 277–282.

[30] Kennedy J, Eberhart R. Particle swarm optimization. In: *Proceedings of the International Conference on Neural Networks (ICNN)*; 1995 Nov 27–Dec 1; Perth, Australia. IEEE; 1995. p. 1942–1948.
[31] Shami TM, Mirjalili S, Al-Eryani Y, et al. Velocity pausing particle swarm optimization: a novel variant for global optimization. *Neural Comput Appl*. 2023;35:9193–9223. doi:10.1007/s00521-022-08179-0
[32] Ke C, Feng YZ, Xian-Feng Y. Hybrid particle swarm optimization with spiral-shaped mechanism for feature selection. *Expert Syst Appl*. 2019;128:140–156. doi:10.1016/j.eswa.2019.03.039
[33] Wang R, Hao K, Chen L, Wang T, Jiang C. A novel hybrid particle swarm optimization using adaptive strategy. *Inf Sci*. 2021;579:231–250. doi:10.1016/j.ins.2021.07.093
[34] Sannigrahi S, Ghatak SR, Acharjee P. Multi-scenario based bi-level coordinated planning of active distribution system under uncertain environment. *IEEE Trans Ind Appl*. 2020;56:850–863. doi:10.1109/TIA.2019.2951118
[35] Abou El-Ela AA, El-Sehiemy RA, Shaheen AM, Eissa IA. Optimal coordination of static VAR compensators, fixed capacitors, and distributed energy resources in Egyptian distribution networks. *Int Trans Electr Energy Syst*. 2020;30:e12609. doi:10.1002/2050-7038.12609
[36] Frahat M, Hatata AY, Saadawi MM, Kaddah SS. Grasshopper optimization-based optimal sizing of DG/DSTATCOM in distribution networks. *Mansoura Eng J*. 2022;47:6–16. doi:10.21608/bfemu.2022.238659
[37] Dash SK, Mishra S. Simultaneous optimal placement and sizing of D-STATCOMs using a modified sine cosine algorithm. In: Das S, Mohanty MN, editors. *Advances in Intelligent Computing and Communication*. Lecture Notes in Networks and Systems, vol 202. Singapore: Springer; 2021. doi:10.1007/978-981-16-0695-3_41
[38] Lasmari A, Zellagui M, Chenni R, Semaoui S, El-Bayeh CZ, Hassan HA. Optimal energy management system for distribution systems using simultaneous integration of PV-based DG and DSTATCOM units. *Energetika*. 2020;66:1–14. doi:10.6001/energetika.v66i1.4294